7 The $\pi^+ \to e^+\nu_e$ / $\pi^+ \to \mu^+\nu_\mu$ branching ratio

P. Robmann, A. van der Schaaf and P. Truöl

in collaboration with: University of Virginia, Charlottesville, USA; Institute for Nuclear Studies, Swierk, Poland; JINR, Dubna, Russia; PSI, Villigen, Switzerland and Rudjer Bošković Institute, Zagreb, Croatia

(PEN Collaboration)

The branching ratio $B \equiv \Gamma_{\pi^+\to e^+\nu_e}/\Gamma_{\pi^+\to\mu^+\nu_\mu}$ in lowest order is given by the product of a phase-space factor and a helicity factor:

$$B \simeq \left(\frac{m_\pi^2 - m_e^2}{m_\pi^2 - m_\mu^2}\right)^2 \times \frac{m_e^2}{m_\mu^2}$$
$$= 5.4869 \times 2.3390 \times 10^{-5} = 1.2834 \times 10^{-4}.$$

Uncertainties associated with the hadronic corrections cancel and radiative corrections slightly lower this value to 1.2353×10^{-4} [1]. Allowing for flavour dependence of g_ℓ (see graph below) B must be multiplied by g_e^2/g_μ^2.

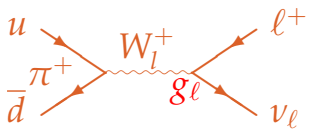

A measurement of B allows sensitive tests of both the $V-A$ structure and the lepton universality of the weak interaction. Until recently the experimental result $1.2312(37)\times10^{-4}$ dated back over thirty years [2] and two new experiments [3] aim at a reduction of the error by almost an order of magnitude. A first result of our PIENU friends, $1.2344\pm0.0023(\text{stat})\pm0.0019(\text{syst})\times10^{-4}$ based on 10% of their data set, was published two years ago [4].

Lepton universality can be tested in other systems too. Results are shown in Tab. 7.1 and 7.2.

TAB. 7.1 – SM and observed values for B_π and B_K

	$\Gamma_{\pi^+\to e^+\nu}/\Gamma_{\pi^+\to\mu^+\nu}$	$\Gamma_{K^+\to e^+\nu}/\Gamma_{K^+\to\mu^+\nu}$
theory	$1.2353(1)\times10^{-4}$	$2.477(1)\times10^{-5}$
experiment	$1.2312(37)\times10^{-4}$	$2.488(12)\times10^{-5}$

TAB. 7.2 – lepton universality tests (τ is the lepton or a lifetime)

decay	g_e/g_μ	g_τ/g_μ	g_τ/g_e
$\pi^+ \to \bar{l}\nu_l$	0.9985(16)		
$K^+ \to \bar{l}\nu_l$	1.0018(26)		
$K^+ \to \pi\bar{l}\nu_l$	0.998(2)		
$\tau^+ \to \bar{l}\nu\bar{\nu}$	0.9998(20)		
$W^+ \to \bar{l}\nu_l$	0.997(10)	1.039(13)	1.036(14)
$\tau \to \pi$ / $\pi \to \mu$		0.996(5)	
$\tau \to K$ / $K \to \mu$		0.979(17)	
$\tau \to e \times \tau_\mu/\tau_\tau$		1.0006(22)	
$\tau \to \mu \times \tau_\mu/\tau_\tau$			1.0005(23)

7.1 The PEN setup

The most expensive component by far is a 3π Sr spherical pure-CsI calorimeter (see Figs. 7.1, 7.2) used to measure positron and photon energies. Pure CsI has its main scintillation decay-time component around 28 ns, much shorter than most other inorganic scintillators.

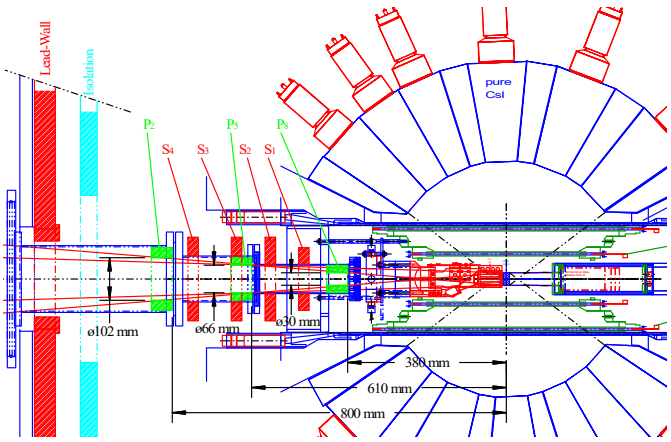

FIG. 7.1 – the PEN setup, $z-y$ cross section.

[1] V. Cirigliano and I. Rosell, JHEP **10** (2007) 5; Phys. Rev. Lett. **99** (2007) 231801.

[2] G. Czapek *et al.*, Phys. Rev. Lett. **70** (1993) 17; D. I. Britton *et al.*, Phys. Rev. Lett. **68** (1992) 3000.

[3] PEN Collaboration, PSI experiment R-05-01 (2005), D. Počanić and A. van der Schaaf, spokespersons; PIENU Collaboration, TRIUMF proposal 1072 (2006), D. Bryman and T. Numao, spokespersons.

[4] A. Aguilar-Arevalo *et al.*, [PIENU Collaboration], Phys. Rev. Lett. **115** (2015) 071801.

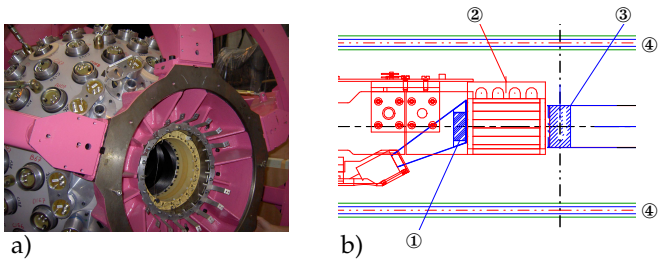

FIG. 7.2 – a) the PEN CsI calorimeter before cabling.
b) target region.
① degrader scintillator, ② mini TPC,
③ target scintillator, and ④ inner MWPC.

PEN took data at PSI during the years 2008 - 2010. Pions from the πE1 beam line stop in a plastic scintillator after having crossed a thin scintillator in an intermediate focus 4 m upstream, a small time-projection chamber (mini TPC) for accurate tracking (see Fig. 7.3) and a degrader scintillator, situated close to the target scintillator. Figure 7.4 shows a distribution of beam counter energy versus time of flight. Time of flight is not only used for particle identification but also for an accurate pion energy determination, event by event, used as input in the target waveform analysis.

Decay positrons from $\pi \to e\nu$ and the sequence $\pi \to \mu\nu$, $\mu \to e\nu\bar{\nu}$, are tracked in two cylindrical MWPCs with analogue cathode strip readout.

The positron energy is determined primarily with the CsI calorimeter. A cylindrical plastic scintillator hodoscope in front of the calorimeter is used both for timing and for particle identification (in particular to separate decay positrons and protons from pion reactions) through $\Delta E - E$.

Whereas the $\pi^+ \to e^+\nu(\gamma)$ decay was recorded with almost 100% efficiency for e^+ emitted in the calorimeter acceptance, the $\pi - \mu$ branch was recorded only for $\Delta t_{\pi e} < 220$ ns. Events with e^+ energies below ≈ 48 MeV were pre-scaled by typically a factor 20.

7.2 Data analysis

The recorded data have been studied in great detail. Calibrations are done and most features observed are reproduced by simulation (see previous annual reports for details).

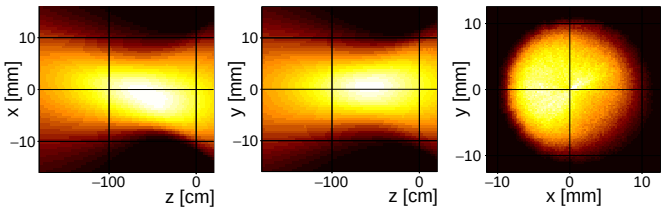

FIG. 7.3 – Mini TPC trajectories. The beam spot, limited by a $\varnothing = 20$ mm collimator, is shifted in x for best suppression of beam e^+ situated further to the left.

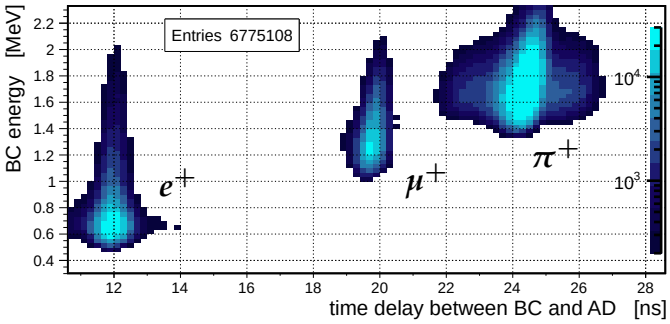

FIG. 7.4 – Beam counter (BC) energy versus time of flight between BC and active degrader (AD) at 75 MeV/c beam momentum. Beam particles (e^+, μ^+ and π^+) are well separated.

Key observables are the $e^+(\gamma)$ invariant mass (μ) and $\Delta t_{\pi e}$. The invariant mass is calculated as the sum of the observed total energy (so e^+ plus γ energies) and observed total momentum (e^+ plus γ momenta, which equals the ν momentum). These observables are reconstructed without individual particle identification, so even for small $e\gamma$ opening angle. The decay sequence $\pi^+ \to \mu^+\nu$ followed by $\mu^+ \to e^+\nu\bar{\nu}(\gamma)$ is characterized by a continuous invariant mass distribution with endpoint m_μ and time delay first rising with τ_π and then falling with τ_μ=2.197 μs.

7.2.1 Target waveform analysis

An important ingredient in the event reconstruction is the (non)observation of a muon signal in the target waveform. The target waveform has contributions from the stopping pion and the decay positron. In most cases there is also the signal from a 4.1 MeV intermediate muon. Figure 7.5 shows target energy distributions for clean $\pi \to \mu \to e$ sequences. Whereas π's and μ's stop in the target (so the distributions represent their kinetic energies) the e^+ energy is the energy loss only which scales with path length and is smeared by Landau fluctuations. Figure 7.6 illustrates for millions of events how π and μ signals merge when the pion decay-time approaches zero.

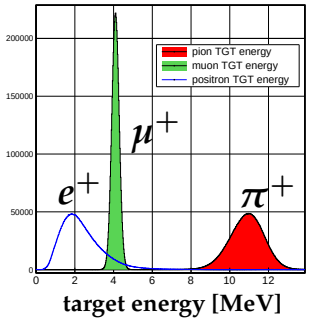

FIG. 7.5 – Target energy distributions for well-separated $\pi \to \mu \to e$ sequences. Secondary μ^+ and e^+ should not be confused with the beam particles in Fig.7.4! Energy quenching has been corrected for. In pion decay at rest muons are monoenergetic with T=4.1 [MeV].

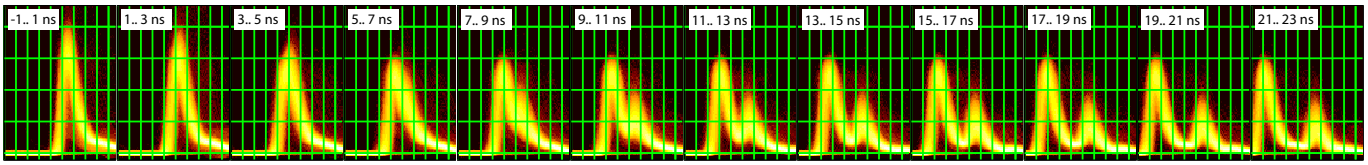

FIG. 7.6 – Filtered $\pi \to \mu$ target signals for windows on the pion decay time (increasing from -1.1 ns to 23 ns) as indicated for events with late positrons.

Figure 7.7 illustrates how the occurrence of an intermediate muon is tested. First the waveform is filtered by multiplication with a vector optimized for optimal almost symmetric output shape. The numerical procedure removes signal tails beyond the scintillator's intrinsic decay-time and reflections caused by imperfect transmission lines. The π^+ and e^+ signals are predicted, based on the full event information. The only free parameter is the location of the 4.1 MeV muon signal. The algorithm gives as output the difference in χ^2 between the hypotheses of a muon or not (see Fig. 7.8). Note that the two event classes can be separated by a factor thousand at least, ten times better than by invariant mass.

7.2.2 Full kinematic reconstruction of $\pi \to e\nu\gamma$

Since the trigger of the experiment, based on the total CsI energy, also selected radiative decays $\pi \to e\nu\gamma$ in the geometric acceptance defined by the CsI calorimeter, the PEN data allow for the first time the analysis of this decay mode in almost the full phase space. The decay $\pi \to e\nu\gamma$ is of interest since, contrary to the inner Bremsstrahlung contribution, the structure-dependent contributions are not helicity suppressed [5].

During 2016 the data analysis was re-organized such that $\pi \to e\nu\gamma$ events can be reconstructed independent of $e\gamma$ opening angle and γ energy. The new approach is based on total energy and total momentum, observed in the full 3π Sr acceptance of PEN which immediately gives the invariant mass (see Fig. 7.9). Combined with the e^+ tracking information a complete kinematic reconstruction is made in the full phase space of the decay, including the region with potential muon decay background which could not be accessed before. Presently the attempt is made to improve the theoretical prediction[3] and to get rid of the stratified sampling.

By the time of writing a full reconstruction of the measurements is in place. What remains to be done is a thorough analysis of the systematic error in B. It is dominated by uncertainties in the low-energy tail of the invariant-

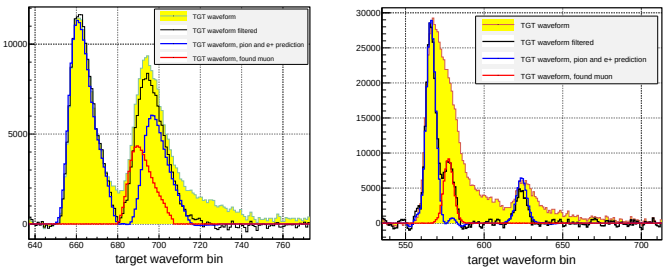

FIG. 7.7 – Two examples of target waveforms and their reconstruction (see text).

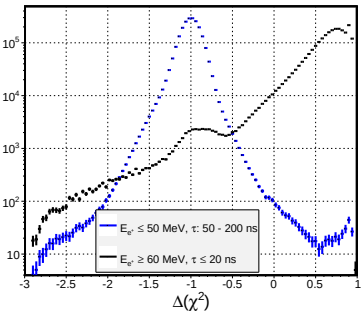

FIG. 7.8 – $\Delta(\chi^2)$ of the target waveform analysis. Events with a muon peak at -1, those without at +1.

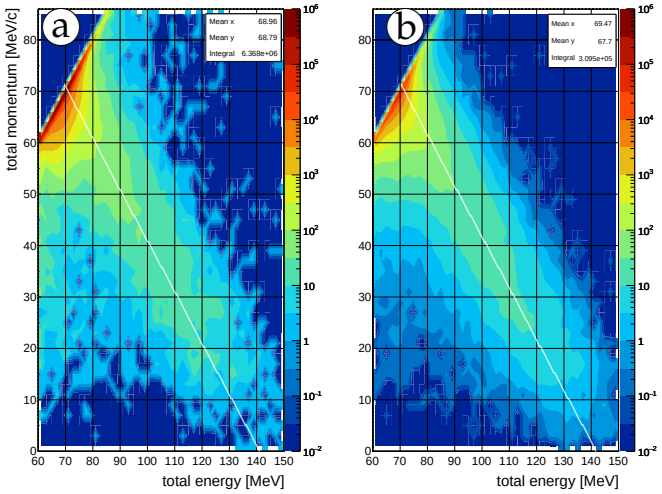

FIG. 7.9 – Distributions of total observed momentum versus total observed energy for events without μ in the target waveform; a) measurement, b) $\pi \to e\nu\gamma$ simulation. In the decay $\pi \to e\nu\gamma$ at rest the total momentum is equal to the ν momentum, so $E + pc = m_\pi c^2$ (white lines). In the present simulation events with $E \approx pc$ (low γ energy and small $e\gamma$ opening angle) have been suppressed.

[3] We acknowledge advice by Gino Isidori in these matters.

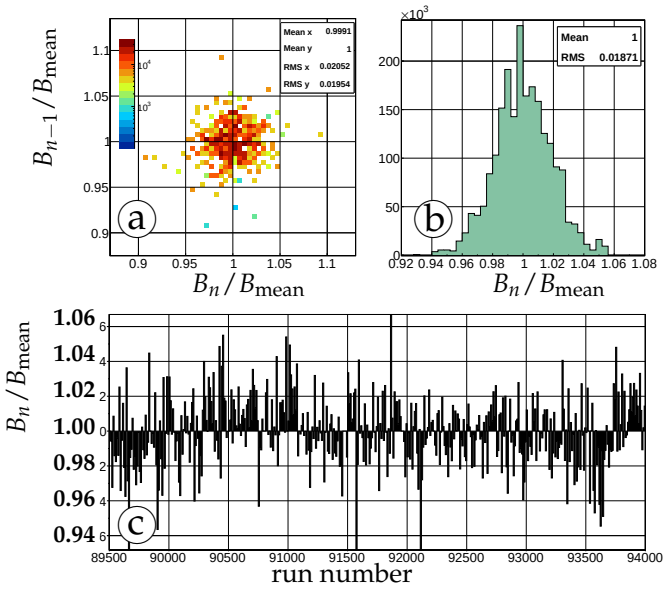

FIG. 7.10 – B, normalized to its mean value, during 2009 for six hour beam periods. a) correlation between consecutive measurements of B_n/B_{mean}. b) distribution of B_n/B_{mean} weighted with $N_{\pi\to e\nu}$ observed during the measuring period. c) B_n/B_{mean} versus run number.

mass distribution which ultimately relies on simulation. The uncertainty in the fraction of $\pi^+ \to \mu^+\nu(\gamma)$ decays within the chosen $\Delta t_{\pi e}$ window is minimized by choosing a window corresponding to the situation in which the event rate is equal at both ends. For a 100 ns wide window this happens for 81.4 - 181.4 ns.

Figure 7.10 gives a feeling of the PEN data quality. Shown are simple determinations of B during the first year of data-taking, corresponding to roughly one third of the full data set. For beam periods of ≈ 6 hours B is determined in a simple cut analysis of invariant mass, $\Delta t_{\pi e}$ and $\Delta(\chi^2)$ of the target waveform. The statistical error of the full data set as deduced from Fig. 7.10 b) is below 0.05%.

FIG. 7.11 – PEN crew solving problems in a bar in Charlottesville. Left to right: Charlie Glaser, Anthony Palladino, Andries van der Schaaf, Mike Vitz, and Martin Lehman.

The final results of PEN are in Virginia hands after the old man on Fig. 7.11 retired on April 1st 2017.

[5] For details see the 2013 PEN report http://www.physik.uzh.ch/reports.shtml.